International Journal of Innovative Research & Growth
A Peer Reviewed Journal
E-ISSN: 2455-1848
homepage: http://www.ijirg.com/ijirg/
Volume: 13 Issue: 4, October 2024

Pulmonary Lung Nodule Identification Using 3D Deep CNN

Ramveer Gurjar[1*], Ajitesh Singh Baghel[2]
[1]Research Scholar, Department of Computer Science & Application, Swami Vivekanand University Sagar-470228, M.P., India
[2]Associate Professor, Department of Computer Science & Application, Swami Vivekanand University Sagar-470228, M.P., India
E-mail: rsgurjar12@gmail.com
* Corresponding Author

Article Info
Received 18 August 2024
Received in revised form 22 September 2024
Accepted for publication 12 October 2024
DOI: 10.26671/IJIRG.2024.4.13.104
Cited as
Gurjar, R., Baghel, A. S. (2024). Pulmonary Lung Nodule Identification Using 3D Deep CNN. *Int J Innovat Res Growth*, 13, 146-155.

Abstract

The main aim of the study is to identify CT Images based pulmonary nodule using 3D Deep Convolutional Neural Network. Many studies have developed novel strategies for detecting PNCs, but the intricacy and diversity of pulmonary nodules make this a hard endeavor. CA detection identifies the location of lesions. This approach is useful for more thorough investigations of medical photographs. Medical photos are employed in scientific research to discover adaption signals. The picture quality may be assessed using the SN (signal to noise) ratio and signal detection in an image. Furthermore, a 3D DCNN classifier was successful in reducing false positives. As a consequence, the suggested model performed well during validation testing on the LUNA 16 dataset. As a result, the suggested model is regarded as an effective clinical tool for screening lung cancer.

Keywords: - Lung Nodule Segmentation, ResNet, 3D Deep Convolutional Neural Network, PNCs.

1. Introduction

For early-stage diagnosis of lung cancer, automatic segmentation of lung nodules is an important step. We proposed a generative adversarial network-based approach for lung nodule segmentation. This chapter describes CT Images based pulmonary nodule identification using 3D Deep Convolutional Neural Network.

One of the primary causes of cancer death is lung cancer, which has a high rate of morbidity and mortality. A recent study found that just 10-16% of lung cancer patients survive. It also indicates that 70% of patients receive a diagnosis with a new kind of cancer for which there is no viable therapy. Early detection of pulmonary nodules is critical for increasing patients' 5-year survival rates to 52%.

According to Fernandez-Cuesta et al. (2016), early detection of lung tumors may improve patient survival rates. Chest x-ray imaging is used to detect lung tumors early on. It aids in determining if the lungs are working properly (or not).

Soltani-Nabipour et al. (2020) found no nodules in normal lung function photographs, however diseased lungs clearly showed nodules. The involvement of nodules does not usually indicate a lung malignancy. Other infections, such as TB or pneumonia, may also occur. The picture is made up of pixels organized in columns and rows according to a matrix.

Image intensity can be used to depict pixel images. The images are categorized into three categories. They include binary, grayscale, and RGB (red, green, and yellow) images. The binary picture is made up of two colors, black (0) and white (1). In the grayscale picture, each pixel has only one intensity. It may be identified using red, blue, and green. The image's pixel intensity ranges from 0 (black) to 255 (white). RGB images can identify every color that humans can see. Each pixel in an RGB picture has three fundamental colors. The image's base color ranges from zero to 255.

Many studies have developed novel strategies for detecting PNCs, but the intricacy and diversity of pulmonary nodules make this a hard endeavor. CA detection identifies the location of lesions. This approach is useful for more thorough investigations of medical photographs. Medical photos are employed in scientific research to discover adaption signals. The picture quality may be assessed using the SN (signal to noise) ratio and signal detection in an image. CA detection is a

pipeline technique that includes image pre-processing, cancerous nodule identification, false positive reduction, malignancy reduction, and malignancy prediction (Kasinathan et al. 2019).

This pipelining technique comprises several steps, which need labeled information throughout the training phase. In recent years, great progress has been achieved in the field of lung tumor categorization through the use of machine learning approaches. Machine learning (ML) is a subset of artificial intelligence (AI) that allows the system to grow and learn from experience without being designed.

Giger et al. (2018) describe how ML methods employ information to learn and discover exact outcomes. ML focuses mostly on the progress of a computer program that reads data and utilizes it to learn from it. The number of categories in the ML process varies. It is used in picture classification with a high-dimensional training dataset. It assigns 0% probability and is unable to make predictions. Huang, et al. (2018).

Lung tumor categorization is a popular application in machine learning. It determines if a patient has lung tumor illness or not. ML methods can do major tasks, but they fall short of mimicking human intellect. These disadvantages can be mitigated by implementing deep learning. Deep learning is a subset of machine learning.

Deep learning is the process of categorizing, grouping, and predicting objects using a neural network that has been trained on large quantities of data. It has its origins in neural networks. Neural networks are collections of algorithms built loosely after the human brain and meant to identify patterns. Deep learning generates multiple layers of neurons in a bid to learn structured representations of large amounts of input layer by layer Jiang et al. (2019).

Deep learning algorithms may be taught directly using training data without the need for pre-processing, resulting in clear and noise-free samples. Deep learning algorithms can learn from noisy data. Pre-processing procedures are mostly utilized in the prediction and classification processes to increase the algorithm's accuracy.

CN networks include massive information applications, including periodic data and graphics. The training procedure primarily involves network feature extraction and weight determination. This CN network can automatically extract data or pictures. It cannot utilize generic matrix multiplication, but instead use the convolution approach to retrieve the lung tumor picture. The feature extraction allows the input image and extracts the output image using neural networks.

Convolutional layers were employed to convert the lung tumor picture. CN networks frequently need health care applications to automatically recognize aspects linked to data timing and image frequency. The deep CN network receives information based on the fault's diagnosis and categorization using the feedback loop approach. It leverages numerous information datasets. Yu et al. (2019).

The CN network is broadly split into three categories. There are three types of CN networks: one-dimensional, two-dimensional, and three-dimensional. The 1D CN network model retrieves characteristics from the underlying structure through displays or data sequencing. This may be accomplished by extracting features from big datasets. This approach is utilized for time series analysis of sensor information and analyzing signal data over a set period of time. The 2D CN networks may scan an item using a filter to check the pixel size at a time, for example, 55 (or) 33 pixels. The pixel value with dot product in the filter window is computed using the convolution procedure.

The 3D CN networks is the sophisticated model that integrates objects using color images to quantify the low-level feature extraction. Zhao, et al. (2018). It includes datasets with a 3D filter that transfers 3D (u, v, and w). The output form is a three-dimensional volume space, such as a cuboid (or) cube shape. This technique is effective for recognizing items like 3D medical photos and films. It is also utilized for 2D pictures, such as in the photo identification process. The three dimensions of data, height, depth, and length, are employed in 3D CN networks to generate three-dimensional activation maps.

Neural network-based deep techniques can handle large amounts of input data. The 3D CN networks may be used to classify lung tumor images. The fundamental goal of the max pooling approach is to minimize the dimensionality of input data, such as images and videos. This lowers the computational cost by lowering the number of parameters required to perform translation invariance-based internal analysis. The maximum pooling is obtained by adding a filter in the nonoverlapping subregions. Thakur et al. (2020).

DCNN is an advanced approach for analyzing lung tumor images to determine whether they are nodules or not (Dietz et al., 2019). This DCNN approach is likewise similar to an artificial neural network. It is composed of an input layer, many hidden layers, and an output layer. The buried layer plays a crucial role in detecting nodules in images.

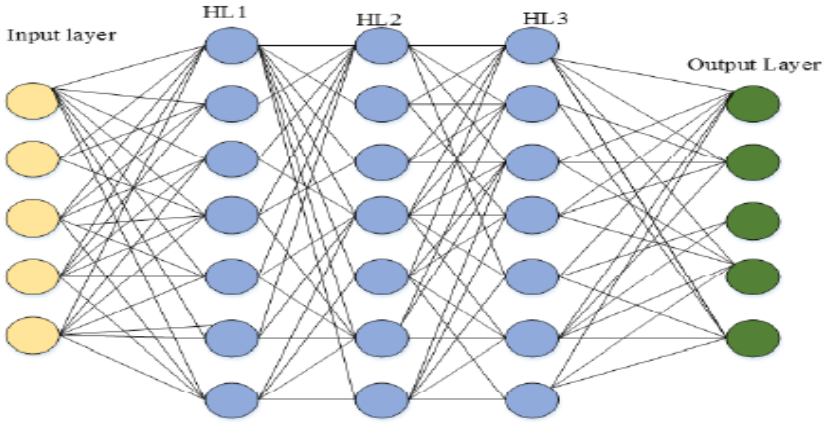

Figure-1 Block diagram of DCNN.

Figure 1 depicts the fundamental block diagram of DCNN with three layers. The DCNN is a sophisticated approach that includes an input layer, several hidden layers (HL1, HL2, and HL3), and an output layer. Initially, the characteristics are sent to DCNN for hidden layer classification. The hidden layer comprises neurons with input information, and it serves as the foundation for the classification process. DCNN is used to get both lateral genetic (LG) and horizontal genetic (HG) transmission of pictures. Each convolutional layer's input channels include filters for analyzing local connection patterns. The convolutional filters are used to collect channel-specific data inside local fields. In this study, the Squeeze and Excitation (SAE) block is presented to improve channel relationships.

The SAE model is used to increase network representational power across channels. Yu et al. (2019) presents a feature recalibration approach for improving network power. Using this strategy, it may acquire global data to discover relevant information while ignoring less helpful data. The excitation mechanism incorporates sample-specific activations for each channel using a gating approach linked to channel dependency. Based on the quality result, the feature map is re-evaluated in the SAE block before being sent immediately to the next layer.

The SAE network has several collections of SAE blocks that can replace the original block in the structure. In the following layers, the SAE block responds to various input images in a certain way. Finally, the feature recalibration of SAE blocks may be applied over the whole network. DCNN is not an easy process, however the SAE block aids in the diagnosis of lung tumors using several layer configurations and additional hyper parameters. The computational cost and model complexity are marginally increased in SAE blocks. It can be lowered using the LUNA16 dataset after rigorous review.

The dataset of LUNA16 is a type of publicly available dataset for identifying pulmonary nodules. This dataset removes CT image thickness more than 3mm also filters annotated nodule size less than 3mm. The nodule size ≥3 is represented as positive and the nodule size ≥3 is denoted as negative. In order to obtain better results, LUNA16 dataset is used for classification of lung tumor image. The dataset contains many numbers of 3D residual blocks.

2. Proposed Methodology

This section discusses a unique DCNN-based CAD model for recognizing pulmonary modules in CT images. The suggested approach aims to provide a promising outcome for identifying lung nodules. The suggested model's implementation is divided into three parts. Initially, the detector and classifier in the proposed model are entirely based on 3D DCNN, which is suitable for volumetric medical image processing. The second step is nodule candidate identification, which involves a 3D Region Proposal Network (RPN) based on a U-Net-like architecture trained using the OHNM technique. In the third phase, the SE-ResNet module is introduced to speed up the training process and improve the accuracy of pulmonary nodule identification.

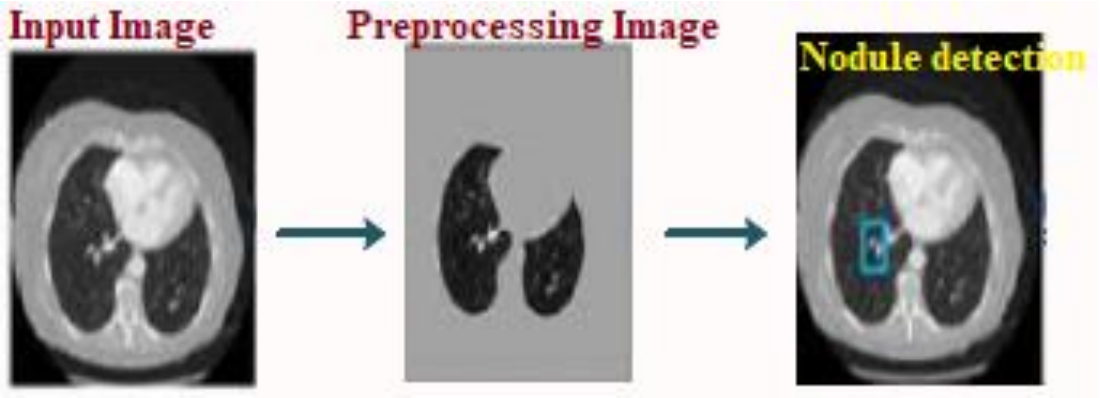

Figure-2 Classical pulmonary nodule detection.

Figure 2 depicts the conventional lung nodule identification technique. Figure 3 shows some of the classic lung nodules.

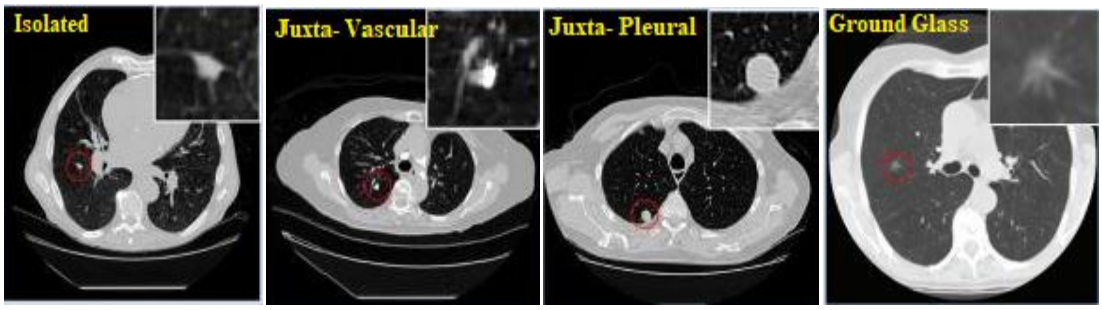

Figure-3 Traditional pulmonary nodules.

As previously stated, the majority of automated CAD models include both nodule candidate detection and false positive reduction. Classical models frequently need handcrafted characteristics such as pixel thresholding, voxel grouping, and morphological characteristics.

3. Dataset

Kopelowitz et al. (2019) assessed the suggested model using the LUNA 16 dataset, which included 1186 nodules and 88 CT images in total. The LUNA 16 dataset is derived from the huge public LIDC-IDRI dataset. Each picture represents a slice that is 512 × 512 in size and has a thickness of less than 2.5 mm. Scans with missing slices and slice thicknesses more than 2.5mm are acceptable. In LUNA 16, the contributors create their algorithm and input their predictions on 888 CT images. One of the two trajectories include:

(a) The whole nodule detection trajectory where an entire CAD system has been accomplished.
(b) False positive reduction trajectories in which a given nodule contender set is classified.
Figure 4 presents the five different chest images obtained from LUNA 16 dataset.

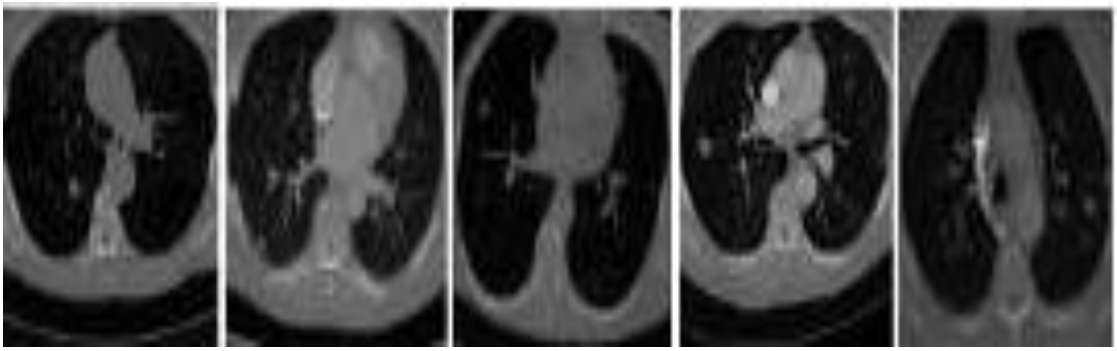

Figure-4 Five different chest images obtained from luna 16 dataset.

Besides, the pulmonary module annotations in the dataset have acquired through a two-stage image annotation process carried out by four skilled radiologists. Figure 5 presents the sample CT images with nodules.

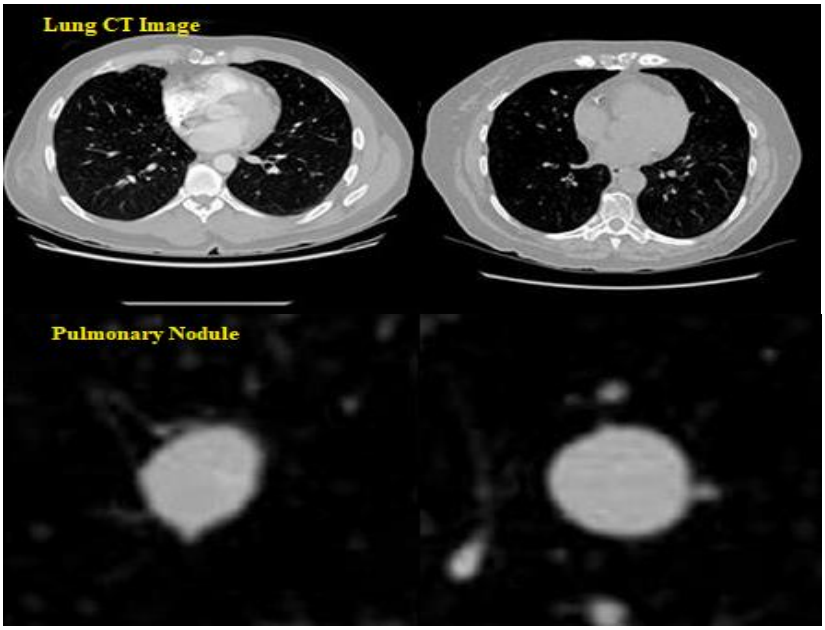

Figure-5 Sample CT images with nodules.

All radiologist's annotations lesion they detected as nodules fewer than 3mm, non-nodules as well as modules greater than 3mm 11. Bhandary et al. (2020). The situation standard of LUNA 16 challenge includes each module ≥3mm acknowledged by minimum three of the four skilled radiologists.

3.1 Nodule Candidate Identification

The goal of detecting nodule candidates is to identify them with greater sensitivity while simultaneously limiting the total number of nodule candidates. Motivated by the success of object detection using deep learning, bronchial nodule detection may also modify a one-stage object detection model based on CNN. According to the inquiry and experiments, the suggested model has modelled the detection structure based on the 3D SE-ResNet Module, resulting in improved performance.

3.2 Res Nets

ResNets' policy is motivated by VGG-19. It is regarded as one of the most complex proposed structures for ImageNet (image classification and object detection problem). Generally, in CNN, various layers are linked and taught to do distinct

tasks. At the conclusion of each layer, the network might learn different degrees of characteristics. In ResNet, the layer known as convolutional has roughly 33 filters. ResNet layers have a similar number of filters, resulting in an output feature map that is of comparable size. Furthermore, if the size of the output feature map is half, the number of filters is quadrupled to accommodate the temporal complexity of each layer. ResNet downsamples directly via convolving layers, with a stride of 2. ResNet terminates with a global average pooling layer and a Softmax-activated fully linked layer. Figure 6 depicts the block diagram of the ResNet module.

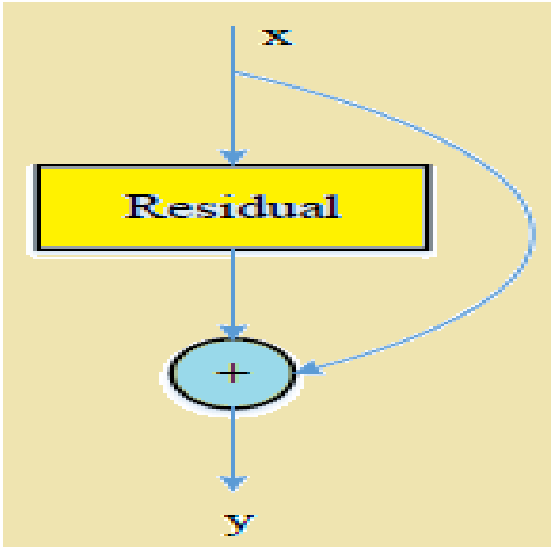

Figure-6 Block diagram of ResNet module.

In ResNet, the residual learning has been simply inferred as subtraction of input features learned from that layer. To execute this, employing shortcut connections to all the pairs of 33 filters, straightly relating the input of l^{th} layer to l+y)th. The rationale for skipping layers is to avoid the issue of disappearing gradients by reusing the activations from the preceding layer until the layer closest to the newest one has learned its weight. During network training, the weights may be adjusted to enhance the layer following the current layer while also muting the preceding layer. Furthermore, the network is easier to train than the DCNN. In addition, the ResNet can address the issue of accuracy decay.

3.3 Squeeze and Excitation Blocks with ResNet

Recently, it was shown that integrating Squeeze and Excitation (SE) blocks with the ResNet model resulted in significantly improved performance in identifying lung nodules. The SE-ResNet architecture was created by stacking SE blocks on top of one another. SE-ResNet generalizes much better across lung tumor datasets. The following equation expresses the specified transformation for either a set of convolution or convolution:

$$A_{ut}: \mathrm{Y} \rightarrow \mathrm{Z}, \quad \mathrm{Y} \in S^{X_0 x I_0 x D_0}, \quad \mathrm{Z} \in S^{X \times I \times D} \qquad (1)$$

where X represents width, I indicates height, D represents the number of channels after using Y and Z as input and output feature maps, and t denotes the reduction ratio. Initially, the input feature Y was sent into the squeeze operation, which is used to average the feature maps throughout the spatial plane. After that, two completely linked layers with Sigmoid and ReLU activations were used independently to execute excitation operations.

3.4 3D SE-ResNet Module

The 3D SE-ResNet module consists of two features. One of the aspects is squeeze and stimulation, while another is residual learning. The squeezing and excitation performances are mostly utilized for adaptive feature reevaluation. The residual learning includes a reuse feature based on a 3D Deep CN network. The squeeze and excitation approach improves the network's power usage. It supports dynamic channel-based feature reconsideration between channels. To improve pulmonary node proof of identity, the image processing work is performed utilizing the 3D SE-Res Net approach. The network is used to improve feature channel selection throughout the re-evaluation process. The squeezing and excitation concept increases capacity across the network. The volumetric CT scan-based pulmonary module identification is a type of 3D item identification system that employs a novel 3D SE-ResNet technique that can be assessed by converting the 2D squeeze and excitation version with the residual model to a 3D model. The newly suggested 3D SE-ResNet approach extracts more valuable 3D photos than 2D ones.

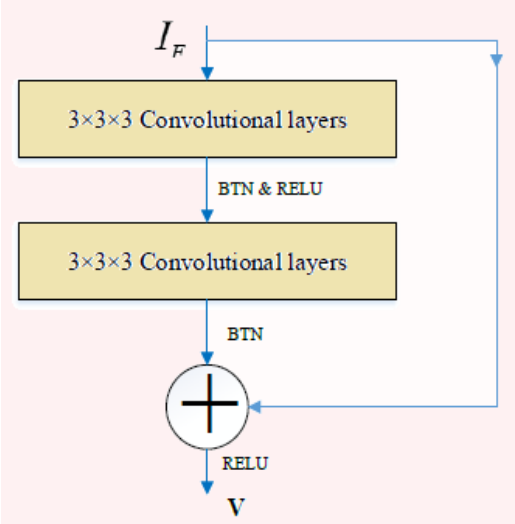

Figure-7 3D ResNet module.

Figure 7 depicts the 3D RN module built on typical neural networks. Each layer in common neural networks feeds straight into the subsequent levels for execution. Based on this 3D RN module, each layer links straight to the next layer while skipping 2-3 hops for improved identification. The basic aim of neural networks is to perform universal processes, and the accuracy grows as the number of layers increases. In this case, BN (batch normalization) improves the training process of the lung tumor classification picture, lowering the total error rate while increasing accuracy.

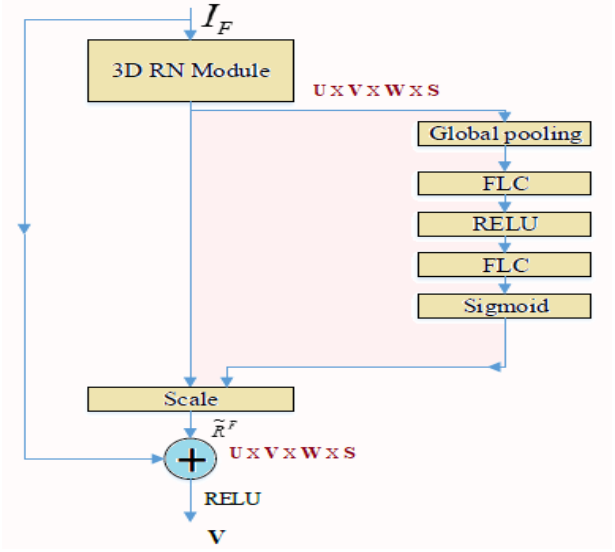

Figure-8: 3D SE-ResNet module.

Figure 8 depicts the proposed 3D SE-ResNet module paired with a deep network to study lung tumor categorization. The FLC (fully connected) is an artificial neural network that links one layer of neurons to the next layer of neurons. The suggested model primarily concerns the identification of pulmonary nodules using the RELU technique. It can learn characteristics with strong discriminating potential to deliver superior outcomes.
The feature selection of the images can be derived in the following equation.

$$R^F = \mathrm{R_M}\ (\mathrm{I_F}) \qquad (2)$$

Here, the input feature is denoted as I_F, the function of residual mapping is represented as R_M, and the residual feature is shown as R^F.

$$T_S = R_{SEQ}\ (R_S^F) = \frac{1}{U \times V \times W} \sum_{x-1}^{U} \sum_{Y-1}^{V} \sum_{x-1}^{W} R_S^F(x, y, z) \qquad (3)$$

Where, T = $[T_1, T_2, T_3 \ldots\ldots T_s]$and T_s is denoted as the s^{th}element of S T$\in L^s$ The squeeze function is denoted as R_{SEQ}, which combines the total spatial data using global average pooling to obtain channel based statistics. The number of channels in the residual mapping is represented as S. The spatial dimension of $R^F$is given as U×V×W. The feature map of s^{th} channel based residual feature R^F can be derived as

$$R_s^F \in L^{u \times V \times w}$$

$$\mathrm{b} = R_{EX}\ (\mathrm{T,W}) = \mathrm{a}\ (W_2 \beta (W_1 \mathrm{T})) \qquad (4)$$

Here, the excitation factor is denoted as R_{EX}which can obtain scale values b=$\in L^s$for channel based residual feature. The factors of the fully connected layers are denoted as $W_1 \in L^{s\times\frac{s}{1}}$ and $W_2 \in L^{s\times\frac{s}{t}}$. The rectified linear unit is represented as β and the sigmoid factor represents as α. The reduction ratio is fixed at t=16 for minimizing the computational costs.

$$\widetilde{R_s^F}=R_{scale}(R_s^F,b_s) = b_s.\ R_s^F] \quad (5)$$

$$\widetilde{R^F}= [\widetilde{R_1^F}, \widetilde{R_2^F} \dots\dots\dots \widetilde{R_s^F}] \quad (6)$$

Here, the learned scale value $b_s$and the feature map $R_s^F \in L^{U\times V\times W}$ for channel wise multiplication are referred to as $R_{scal}(R_s^F, b_s)$. The s^{th} channel significance is derived using scale value b_s. Once, the squeeze and excitation processarecompleted, the residual feature calibration $\widetilde{R^F}$can be achieved.

$$V=\beta\ (\widetilde{R^F} + I_F) \quad (7)$$

Where, the element wise addition process and the shortcut connection are obtained using formulation $\widetilde{R^F}+I_F$ The output feature for the rectified linear unit β can be denoted as V.

To extract pulmonary nodule characteristics, the suggested 3D SERN approach may be improved using a deep network and the Deep CN network. It also serves to highlight the characteristics of information nodules. The suggested 3D SERN modules have strong discriminating capacity and improved characteristics, making them useful for diagnosing pulmonary nodules.

3.5 Architecture Identification Process

The 3D RP (region proposed) network uses several scale anchors to identify the item. The U-net architecture uses a combination of deep layers and superficial characteristics to bypass connections. This method is useful for identifying multi-scale nodules.

Figure 9 depicts the construction of a 3D CNN for identifying lung nodule candidates. Here, the CT image is used as the network's input. The feed forward pipeline has two convolutional layers with a kernel size of 3×3×3. The suggested 3D SE-ResNet blocks model interleaves four different 3D max pooling layers. Initially, the two 3D SE-ResNet modules include 3D SE-ResNet blocks, followed by three modules.

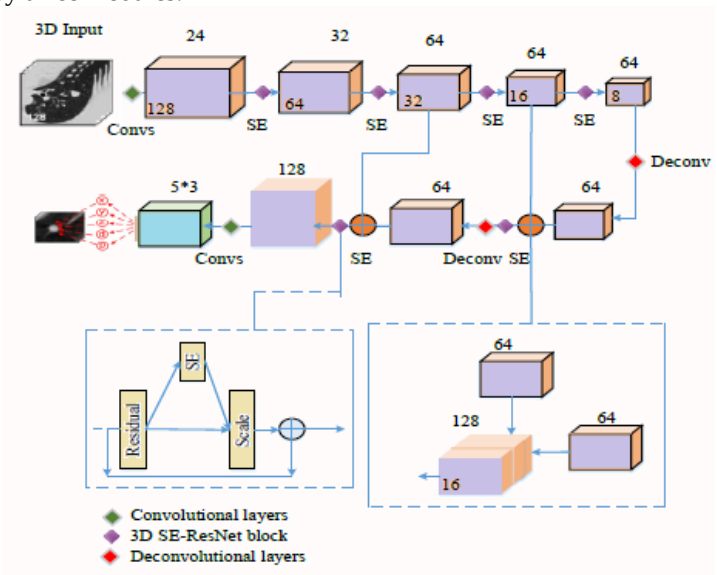

Figure-9 Architecture of 3D CNN for pulmonary nodule.

The backward route procedure includes two 3D SE-ResNet blocks and two de-convolutional layers with stride and kernel sizes of two. Each de-convolutional method combines feed forward path-based feature maps with the associated layers. This block is followed by dropout with a probability of 0.5, as well as two convolutional blocks with a kernel size of 2. The anchors of three various sizes can be used to create the final feature map for producing object suggestions. Each anchor size contains 5*1vector that denotes the object score, diameter and location (i, j, k). The nodule distributions of sizes with anchors are 5 mm, 15 mm, and 35 mm

Each anchor box with a binary class label can be allocated to an Intersection Over (IO) union-based target nodule. The anchor box for IO union exceeds 0.5, indicating positive samples. The anchor box for IO union is less than 0.02 value, which is considered a negative sample. Rener et al. achieved multitask learning using an RPN model. The RPN model is best suited for ablation studies to increase identification accuracy, regression learning, and classification learning, however the RPN technique has a larger multitask learning loss. In order to minimize multitask loss, this model involves regression loss for nodules (

$\alpha_\delta^*= \left(\frac{i-i_a}{n_a}, \frac{j-j_a}{n_a}, \frac{k^*-k_a}{n_a}, \right) \left(\frac{n^*}{n_a}\right)$, anchor box-based classification loss and size of the nodule (n).

The multi-task function for each labeled nodule is derived by the following equation.

$$N(m,a) = \emptyset N_{CLA}\ (m,m^*) + m^*\ N_{REG}\ (\alpha_{\delta,}\alpha_{\delta}^*) \quad (8)$$

Where, the label value for an anchor box is denoted as m^*. The predicted value for an anchor box is represented as m. The positive sample of the label value is m^*=1 and the negative sample of the label value is m^*=0. The four parameters of the ground truth bounding box and the predicted bounding box are denoted as a_δ a and $\alpha^*\delta$, respectively. The weight factor for the two loss terms is represented as ∅=0.5. The classification loss $N_{CLA}(m,m^*)$ can be evaluated using binary cross entropy loss function. The regression loss $N_{REG}\ (\alpha_\delta\alpha_\delta^*$for location information can be derived using smooth N1 loss function. Based on the above equation, the positive sample labeled as is considered for regression loss.
The combined regression loss of location data can be denoted as follows.

$$N_{REG}(\alpha_\delta, \alpha_\delta^*) = \sum_{\delta\in\{i,j,k,n\}} SM_{N1}(\alpha_\delta - \alpha_\delta^*) \quad (9)$$

$$SM_{N1}(i) = \begin{cases} 0.5i^2, if|i| < 1 \\ |i| - 0.5, others \end{cases} \quad (10)$$

The four factors of the ground truth bounding box are shown in the following equation.

$$\alpha_\delta^* = \left(\frac{i^*-i_a}{n_a}, \frac{j^*-j_a}{na}, \frac{k^*-k_\alpha}{n_a}, log\left(\frac{n^*}{n_a}\right)\right) \quad (11)$$

The four factors of the predicted bounding box are derived in the following equation.
Here, the side length and the coordinates of the predicted bounding box are denoted as (i, j,k,n),the ground truth bounding box parameters are shown as (i^*, j^*, k^*, n^*). The anchor bounding box parameters are represented as (i_a, j_a, n_a).
During the nodule applicant detection stage, it was discovered that the negative samples outnumber the positive samples. While many of the negative samples were easily identified, a few hard negative samples remained unidentified. The hard negative samples contained the most valuable data, while the easily identified samples assisted in analyzing the differences between the negative samples. During the HNM process, the network generates many proposed bounding boxes based on different confidence metrics. In the suggested model, negative samples S can be picked at random from the candidate pool. The negative samples for the classification confidence score-based sigmoid function are listed in descending order. The initial samples are then recognized as hard negatives. The loss computation excludes all other negative samples.

3.6 Pre-Processing

Pre-processing is a key step in improving the accuracy of the system. This pre-processing procedure improves picture quality by sharpening it in order to remove the noise present in the lung tumor image. The pictures acquired from the LUNA 16 dataset include MR images classified into four classes depending on tumor development and intensity. MR pictures are mostly composed of noise caused by temperature, sensors, and lightning. The noisy photos are pre-processed with filtering. This filtering mechanism is also known as the Extended Adaptive Wiener (EAW) filter. The EAW filter improves image quality by eliminating noise and protecting edge data. The suggested approach incorporates the dispersion index, which is based on an investigation of locating clustered and scattered existences. The pixel location of the input picture l P is represented by 1 P and 2 P, respectively. The noise-added picture is recovered and smoothed to get the highest quality image. Equation 4.12 denotes the dispersion index.

$$D_{IN} = \frac{r_{no}^2}{\lambda} \quad (13)$$

Here, r_{no} denotes the noise variance and λ represents the mean value. The typical AW filter with dispersion noise is obtained, and the equation is represented as follows.

$$S_f\ [P_l(P_1, P_2)] = \lambda + \frac{D_{IN} - r_{no}^2}{D_{IN}} = [P_l(P_1, P_2) - \lambda] \quad (14)$$

Where, μ is the mean and r_n is noise variance.
The aforementioned AW filter equation is simplified, and the newly derived EAW filter equation is incorporated into the equation.

$$S_f\ [P_l(P_1, P_2)] = [P_l(P_1, P_2) - \lambda\left(\frac{r_{no}^2}{r^2}\ [P_l(P_1, P_2) - \lambda]\right) \quad (15)$$

The above equation clearly represents the quality of the supplied image. In addition, the MR images contain speckle noise, which is eliminated during the EAW filtering process. It improves both the texture and contrast images.

3.7 Segmentation

The LUNA16 dataset is utilized in lung tumor image segmentation to identify lung area masks. Dilation and convex hull are used to include all nodules in the procedure for segmentation. Deep CN network-based lung tumor image segmentation extracts 2D slices from 3D information and reconstructs the 3D volume of data. Essentially, 3D lung images are stored in NIT (neuro-imaging informatics technology) format. The windowing filters protect the RI (region of interest). The

processing of pictures is used to segment CT images so that sick and healthy instances may be identified. To achieve an effective segmentation procedure, the background objects and skeletal structures in a picture are sliced using a basic thresholding method using image intensity. The dilation and erosion approach is utilized to isolate the lung tumor picture from other background objects using morphological processes. The structural element process can fill any minor gaps in the dilation procedure, whereas the erosion approach comprises the removal of unnecessary items. The binary image output includes "0" values for background and "1" values for lung areas in the CT picture.

The structural element process can fill any minor gaps in the dilation procedure, whereas the erosion approach comprises the removal of unnecessary items. The binary image output includes "0" values for background and "1" values for lung areas in the CT picture. The convex spots represented the red dots that surrounded both corners of the lungs. The Euclidean distances may be calculated using the LUNA16 dataset. Using this dataset model, the segmented lung pictures are reconstructed from the original lung tumor image. Both the original and binary mask pictures are converted using a bitwise technique based on an RGB mask. The clipping process of the final picture normalized values are set to [0,255], and the pixel values are set to [-1200,600]. The non-lung pixels are padded with 170 values. The scanning pictures in the LUNA16 dataset contain varying spatial resolutions and have been resampled to an isotropic resolution of mm.

Following the conclusion of nodule candidate identification, the findings show a large number of false positive readings. The suggested 3D deep CN network-based nodule candidate classification is utilized to accurately distinguish real nodules from a large number of candidates. To limit false positives, numerous pulmonary nodules are diagnosed with a lower false positive rate. The expected coordinates are collected from the detector to extract the candidate crops, which are initially fed into two convolutional layers with kernel size (3) and a max pooling layer. There are three 3D SERN blocks that are used to learn high-level characteristics, each consisting of three SERN modules.

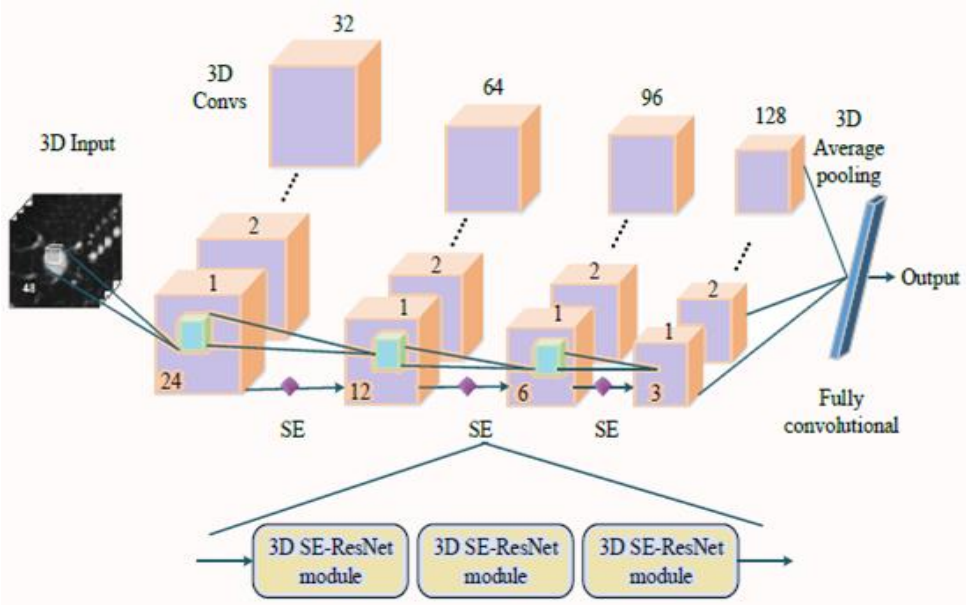

Figure-10 Architecture of 3D DCNN for false-positive reduction.

Figure 10 depicts the construction of 3D DCNNs for false-positive reduction. Every block can be followed by a max pooling layer, whereas the FC layer and 3D average pooling layer are mostly utilized for non-nodule and nodule classification. The probability of dropout layers is set at 0.2. To avoid overfitting, dropout layers are introduced after the FC and max pooling layers. The binary cross entropy is used to assess classification loss. Figure 10 shows the design of 3D DCNN for false-positive reduction, with each 3D SE-ResNet block consisting of three basic blocks.

4. Conclusions

In this paper, an automated CAD model based on deep learning is suggested for detecting pulmonary nodules. The proposed model includes two crucial steps: nodule candidate discovery and false positive reduction, and both phases use SE-ResNet gas to get superior results. To discover the nodule candidates, a 3D RPN-based U-Net architecture was deployed. Furthermore, a 3D DCNN classifier was successful in reducing false positives. As a consequence, the suggested model performed well during validation testing on the LUNA 16 dataset. As a result, the suggested model is regarded as an effective clinical tool for screening lung cancer.

Acknowledgement

The authors are thankful to the referees and the editors for their constructive critical comments for the improvement of the paper.

Conflict of Interest

The Authors declares that there is no potential conflict of interest in this manuscript.

References

[1] Fernandez-Cuesta L, Perdomo S, Avogbe PH, Leblay N, Delhomme TM, Gaborieau V, Abedi-Ardekani B, Chanudet E, Olivier M, et al. (2016). Identification of Circulating Tumor DNA for the Early Detection of Small-cell Lung Cancer. eBioMedicine, 10, 117-123. https://doi.org/10.1016/j.ebiom.2016.06.032
[2] Nabipour, J.S., Khorshidi, A., and Noorian, B. (2020). Lung tumor segmentation using improved region growing algorithm. Nuclear Engineering and Technology, 52(10), 2313-2319. https://doi.org/10.1016/j.net.2020.03.011
[3] Paing, M.P., Hamamoto, K., Tungjitkusolmun, S., and Pintavirooj, C. (2019). Automatic Detection and Staging of Lung Tumors using Locational Features and Double-Staged Classifications. Applied Sciences. 9(11), 2329. https://doi.org/10.3390/app9112329
[4] Giger et al. (2018). Automatic lung field segmentation based on non-negative matrix factorization and fuzzy clustering. In X.-S. Yang, A. K. Nagar, and A. Joshi, Smart Trends in Systems, Security and Sustainability (57-66), Singapore, Springer Singapore.
[5] Han, G., Liu, X., Zheng, G. et al. (2018). Automatic recognition of 3D GGO CT imaging signs through the fusion of hybrid resampling and layer-wise fine-tuning CNNs. Med Biol Eng Comput, 56, 2201–2212. https://doi.org/10.1007/s11517-018-1850-z
[6] Yu, L., Tao, G., Zhu, L. et al. (2019). Prediction of pathologic stage in non-small cell lung cancer using machine learning algorithm based on CT image feature analysis. BMC Cancer 19, 464. https://doi.org/10.1186/s12885-019-5646-9
[7] Zhao, X., Liu, L., Qi, S., Teng, Y., Li, J., and Qian, W. (2018). Agile convolutional neural network for pulmonary nodule classification using CT images. Int J Comput Assist Radiol Surg. 13(4), https://doi.org/10.1007/s11548-017-1696-0
[8] Thakur, S. K., Singh, D. P., and Choudhary, J. (2020). Lung cancer identification: a review on detection and classification. Cancer Metastasis Rev 39, 989–998. https://doi.org/10.1007/s10555-020-09901-x
[9] Dietz, L., Horve, P. F., Coil, D. A., Fretz, M., et al. (2020). Correction for Dietz et al., "2019 Novel Coronavirus (COVID-19) Pandemic: Built Environment Considerations To Reduce Transmission". mSystems, 5(3), 00375-20. https://doi.org/10.1128/msystems.00375-20
[10] Hussain, S., Ameri Sianaki, O., and Ababneh, N. (2019). A Survey on Conversational Agents/Chatbots Classification and Design Techniques. In: Barolli, L., Takizawa, M., Xhafa, F., Enokido, T. (eds) Web, Artificial Intelligence and Network Applications. WAINA 2019. Advances in Intelligent Systems and Computing, vol 927. Springer, Cham. https://doi.org/10.1007/978-3-030-15035-8_93
[11] Bhandary, A., Prabhu, G. A., Rajinikanth, V. et al. (2020). Deep-learning framework to detect lung abnormality–A study with chest X-Ray and lung CT scan images. Pattern Recognition Letters, 129, 271-278. https://doi.org/10.1016/j.patrec.2019.11.013